Interaction distance in the extended XXZ model

Kristian Patrick,[1] Vincent Caudrelier,[2] Zlatko Papić,[1] and Jiannis K. Pachos [1]

[1]*School of Physics and Astronomy, University of Leeds, Leeds LS2 9JT, United Kingdom*
[2]*School of Mathematics, University of Leeds, Leeds LS2 9JT, United Kingdom*

We employ the interaction distance to characterize the physics of a one-dimensional extended XXZ spin model, whose phase diagram consists of both integrable and nonintegrable regimes, with various types of ordering, e.g., a gapless Luttinger liquid and gapped crystalline phases. We numerically demonstrate that the interaction distance successfully reveals the known behavior of the model in its integrable regime. As an additional diagnostic tool, we introduce the notion of "integrability distance" and particularize it to the XXZ model to quantity how far the ground state of the extended XXZ model is from being integrable. This distance provides insight into the properties of the gapless Luttinger liquid phase in the presence of next-nearest-neighbor spin interactions which break integrability.

I. INTRODUCTION

An efficient way for describing a many-body quantum system is by identifying the effective degrees of freedom (DoF) that encapsulate its dominant low-energy properties [1]. In a similar vein to Fermi liquid theory, which applies to weakly correlated systems where the effective DoF are "dressed" versions of the original DoF, it would be desirable to have general techniques to characterize the effect of interactions in general (possibly strongly correlated models), without relying on the specific physics or *exact* mathematical structure (e.g., integrability [2]) of the model. The *interaction distance* [3] provides a systematic measure of the effect interactions can have on a given quantum state of a generic many-body system. In the case of a reduced density matrix (see Sec. II), the interaction distance is determined solely from the entanglement spectrum [4] of the given quantum state; intuitively, it captures the long-distance behavior of a system by identifying the quantum correlations between the emerging DoF. At the same time, it includes information about the structure of the DoF that are dressed by the interactions, thus revealing the short-distance behavior of the model.

The interaction distance compares the correlations of a system to those of chosen free particles, which we assume in this paper to be fermions. Moreover, it identifies the optimal free model closest to the interacting one, thus offering a qualitative and quantitative analysis of the interacting system. Free fermions are a subclass of integrable models that are analytically tractable. Following Baxter's construction of the corner transfer matrix [5], Nishino [6] argued that the 1D integrable models related to the classical eight-vertex model have ground-state correlations that, in the thermodynamic limit, can be exactly described by free fermions [5]. This surprising result has been verified analytically and numerically for several noncritical models [7–9]. This makes the fermionic interaction distance an ideal tool for investigating integrable models, especially away from the thermodynamic limit, where Baxter's results do not apply.

Beyond the interaction distance employed to investigate the behavior of integrable models, it is of interest to also investigate near-integrable models. To characterize this more general class of models, we introduce the notion of "integrability distance"—a distance that measures how far the correlations of the given state of a generic interacting system are from the closest possible *integrable* model of the same size. This measure allows us to identify in principle if a certain physical model is "almost" integrable, thus potentially rendering it amenable to some of the analytical tools of integrability.

We exemplify our approach using the extended XXZ model—a nonintegrable model hosting a Luttinger liquid (LL) phase [10,11]—that has been under intense investigation in recent years. In the integrable limit, properties of the model have been studied extensively via Bethe ansatz [12], leading to exact results for correlation functions both analytically [13] and numerically [14], and density matrix renormalization group (DMRG) [15], either in finite [16] or infinite systems [17,18]. In particular, properties of the gapless LL phase have been tested via explicit calculations of equal-time density response functions [19,20], the density of states at zero temperature [21–23], and power-law decay of correlation functions [24]. Furthermore, it was shown that the LL phase remains stable to a small amount of integrability-breaking next-nearest-neighbor interactions [25–27]. More recently, extensive DMRG studies have mapped out the phase diagram of the extended XXZ model [28], and LL physics has been probed via quantum quenches [29,30].

Here, we demonstrate that a scaling analysis of the interaction distance successfully reproduces the asymptotic free-fermion behavior of the extended XXZ model when restricted to its gapped integrable regime. Moreover, we employ the integrability distance in order to investigate the nonintegrable version of the model at criticality. As the integrability distance is too complex to determine in its full generality, we present a physically motivated simplified procedure that is suitable for describing the extended XXZ model. This distance measures how faithfully the entanglement properties of the ground

state of the (nonintegrable) extended XXZ model can be represented by the LL, thus allowing for a quantitative understanding of the extended model at criticality and potentially tractable analytic treatment.

The paper is organized as follows. In Sec. II, we provide a brief overview of interaction distance and discuss the physical meaning of this quantity, in particular how it can probe both short- and long-distance behavior of the model. In Sec. III, we introduce the extended XXZ model that we employ to demonstrate the diagnostic ability of the interaction distance. Section IV analyzes the integrable XXZ model in terms of the interaction distance. In this section, we identify the asymptotically free behavior of the model in its gapped region and perform a nonperturbative calculation of the interaction distance for the gapless regime. Section V presents the analysis of the extended XXZ model from the perspective of the "integrability distance" that is introduced to measure the closeness of the correlations in the ground state of the extended model to the correlations in the integrable regime. Our conclusions and outlook are presented in Sec. VI.

II. QUANTIFYING THE EFFECT OF INTERACTIONS

This section provides a self-contained overview of the interaction distance, $D_{\mathcal{F}}$, that was originally introduced in Ref. [3] (see also Ref. [31]). The interaction distance is the tool we use in this paper to quantify the effect of interactions on a quantum system. Intuitively, we expect a quantum system to be "noninteracting" if we are able to express its Hamiltonian in a quadratic form, in terms of some suitably defined creation and annihilation operators. However, this requirement may be too stringent for many purposes where the main focus is only on the ground state of the system and a few low-lying excited states. In such cases, we are motivated to redefine "freedom" with respect to the given quantum state, or more precisely its reduced density matrix being approximately expressible in a quadratic form.

A. Interaction distance

We focus on lattice models of interacting fermions, described by creation and annihilation operators, $c_j^\dagger$, c_j. The interaction distance $D_{\mathcal{F}}$ is defined as the trace distance between the density matrix ρ of an arbitrary quantum system and the closest density matrix corresponding to some free system σ, given by [3]

$$D_{\mathcal{F}}(\rho) = \min_{\sigma \in \mathcal{F}} \tfrac{1}{2} \text{tr}(\sqrt{(\rho - \sigma)^2}). \qquad (1)$$

The minimization is performed over all free density matrices σ, which belong to the manifold of Gaussian (free) fermion states $\mathcal{F}$. Specifically, we can write

$$\sigma = \frac{1}{Z_\sigma} \exp\left(-\beta \sum_j \epsilon_j f_j^\dagger f_j\right), \qquad (2)$$

where f_j are some fermion operators, β denotes inverse temperature, and Z_σ is a normalization constant which ensures $\text{tr}\,\sigma = 1$ (we also assume that ρ is normalized in the same manner). Note that f_j are not necessarily the same as the original fermionic operators c_j that appear in the Hamiltonian

describing the system. Moreover, we emphasize that the trace distance is merely one convenient choice for the definition of $D_{\mathcal{F}}$, and other choices like relative entropy [32] can equally well be used.

Expressions Eqs. (1) and (2) can be used in formally the same way in two very different physical contexts: ρ can represent the Boltzmann-Gibbs density matrix of the system, or it can be a *reduced* density matrix, which describes a subsystem A for some (real space) partition of the total system in A and its complement B. In the latter case, assuming that the entire system is in a pure state $|\psi\rangle$, the reduced density matrix ρ_A is defined as

$$\rho_A = \text{tr}_B |\psi\rangle\langle\psi|, \qquad (3)$$

where tr_B denotes the partial trace over the DoF in B. In general, the reduced density matrix ρ_A describes a mixed state, with some effective temperature $\beta = 1$. The negative logarithm of the eigenvalues of ρ_A, i.e., $-\ln \rho_k$, is known as the "entanglement spectrum" [4]. In the case of systems with conformal invariance [33,34] or in topological phases of matter [35], the entanglement spectrum inherits some characteristics of the energy spectrum of the full system, e.g., it reveals the energy excitations at the edge of a topologically ordered system [4]. In this paper, we focus on the reduced density matrix case of $D_{\mathcal{F}}$ for reasons explained in Sec. II B.

We note that the definition of $D_{\mathcal{F}}$ in Eq. (1) appears to require a difficult minimization over all $\sigma \in \mathcal{F}$. Nevertheless, it has been shown that the minimum value can be computed simply from the spectra of ρ and σ [3,36]. Taking this into account, the interaction distance is equivalently given by the simpler expression

$$D_{\mathcal{F}}(\rho) = \min_{\{\epsilon_j\}} \frac{1}{2} \sum_k |e^{-\beta E_k} - e^{-\beta E_k^{\text{f}}(\epsilon)}|, \qquad (4)$$

where we have introduced the notation $e^{-\beta E_k}$ for the kth eigenvalue of ρ, and the eigenvalues of σ are similarly given in terms of

$$E_k^{\text{f}}(\epsilon) = E_0 + \sum_j \epsilon_j n_j^{(k)}. \qquad (5)$$

For every k in Eq. (5), there is a specific pattern of fermionic populations n_j's that take values 0 or 1, and E_0 guarantees the normalization of σ.

The advantage of Eq. (4) is that the minimization is only with respect to the single particle energies $\{\epsilon_j\}$, whose number typically scales linearly with the total size of the system. This is in contrast to the total number of eigenvalues, whose number is exponential in the size of the system or subsystem, depending on whether ρ is a thermal or reduced density matrix. Thus, $D_{\mathcal{F}}$ a diagnostic tool that can be efficiently computed numerically or analytically for any system whenever its energy or entanglement spectrum $\{E_k\}$ is accessible.

B. Short- and long-distance behaviors

The interaction distance $D_{\mathcal{F}}$ in Eq. (1) expresses the distinguishability [32] of the two density matrices, ρ and σ. It has a geometric interpretation as the distance of the density matrix ρ from the manifold $\mathcal{F}$ [31]. Importantly, the optimal free state σ, i.e., the one with the smallest distance from
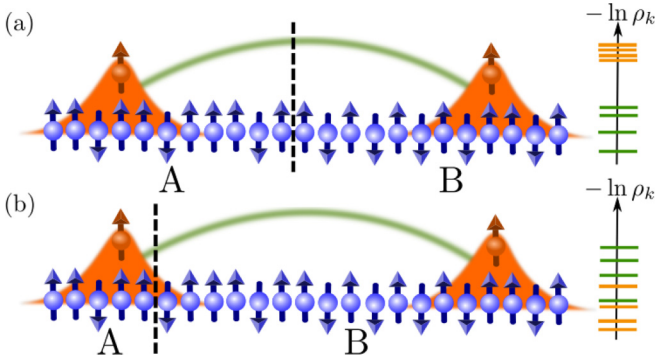
FIG. 1. (a) The dressed degrees of freedom (orange) that effectively describe the behavior of the interacting system are much smaller than the length, L_A, of the subsystem. The low-lying entanglement spectrum is universal and describes the correlations (green line) between such dressed DoF [4] on either side of the partition (black dashed line). The orange part of the entanglement spectrum is associated with the structure of the dressed DoF and it is expected to be separated from the universal green part through an "entanglement gap." (b) The size of the dressed DoF is comparable to the length of the subsystem, which means that partitioning the system would necessarily "cut" through a DoF. In this case, the low-lying entanglement spectrum also probes the internal structure of the dressed DoF.

ρ, does *not* need to be expressed in terms of the original DoF, c_j, that define the Hamiltonian. Moreover, in general, the optimal free state may not be unique, although in many cases it was indeed found to be [3,37]. When ρ is chosen to be the reduced density matrix, $D_{\mathcal{F}}$ measures the distance of the entanglement spectrum, corresponding to the given state $|\psi\rangle$ and the given partition, from the closest possible free-fermion entanglement spectrum, $\{E_k^{\mathrm{f}}\}$, given by Eq. (5). Loosely speaking, $D_{\mathcal{F}}$ measures how much the part A of the system "interacts" with part B [38–43].

An important characteristic of $D_{\mathcal{F}}$ is that it explicitly depends on the partition between A and B subsystems, which can impact its behavior. In the majority of physical systems, the low-energy physics can be described in terms of weakly interacting DoF, which are expressible in terms of dressed original DoF, $U c_j U^{\dagger}$, where U is some unitary transformation. As $U c_j U^{\dagger}$ is a canonical transformation, the resulting operators are still fermionic, but with possibly different characteristics. For example, they might have support on a larger region than just one site j, depending on the action of U on them.

In cases that are amenable to mean-field theory, U can be decomposed into *linear* transformations of c_j operators. In this case, the dressed DoF of the system are the initial fermions, c_j, while the linear transformation determines the quantum correlations between them. However, more complicated choices of U are also possible, which cannot be expressed as linear transformations of the original DoF. Such operators create more complicated types of fermionic DoF that have nontrivial internal structure and may be supported over a larger range of lattice sites; an example is sketched in Fig. 1. In all cases, the correlations between such DoF underpin the low-energy properties of the model. We note that similar ideas have recently been used in the framework of matrix product state methods to construct quasiparticle excitations in various 1D models [44–46].

If the size of the subsystem A is much larger than the typical size ℓ of the dressed DoF (given by the spatial support of the operator U acting on c_j's) as in Fig. 1(a), then the bottom part of the entanglement spectrum captures the correlations between the dressed DoF. The top part of the entanglement spectrum encodes the structure of the dressed DoF isolated from the bottom part by the existence of an "entanglement gap" [4]. As seen from Eq. (4), the contributions from the top part of the entanglement spectrum to the interaction distance is exponentially suppressed. Hence, in this case, $D_{\mathcal{F}}$ probes the large distance behavior, i.e., the correlations between dressed DoF.

If, on the other hand, ℓ is comparable with the size L_A of the subsystem A, this implies that the entanglement partition will necessarily split the dressed DoF. Hence, the interaction distance will probe the physics associated with their internal structure, i.e., short-distance behavior. This is likely to happen at critical points and second-order phase transitions, where the size, ℓ, may diverge. As a result, the behavior of $D_{\mathcal{F}}$ in the two cases may be different, probing the long-distance or the short-distance behavior of the system, depending on its critical behavior or the size of the partition.

From the above discussion, it becomes apparent that $D_{\mathcal{F}}$ quantifies the nonlinear effect interactions may have on the DoF of a system. This distinguishes the interaction distance from other diagnostic tools such as two-point correlations, where the linear and nonlinear contributions in general both contribute. To illustrate this, note that for the XY spin model (which is a special limit of the extended XXZ model, as discussed below), the spin-spin correlation function is given by [47]

$$\langle S_0^z S_n^z \rangle = -\frac{1}{4}\left(\frac{2}{n\pi}\right)^2, \qquad (6)$$

which is valid for *n*-odd. At the same time, the XY model can be easily diagonalized by performing the Fourier transformation, which maps it to free fermions in momentum space. Consequently, we obtain $D_{\mathcal{F}} = 0$ for the XY model for any choice of the partition. This example illustrates that $D_{\mathcal{F}}$ only captures the nonlinear part of the correlations between the original DoF.

III. THE EXTENDED XXZ MODEL

To systematically investigate the effect interactions can have on the low-energy spectrum, we employ a specific example. The systems we have in mind are defined on a lattice, e.g., a system of quantum spins with a local Hilbert space and local (nearest-neighbor) hopping and interaction terms. For concreteness, we focus on the extended XXZ spin-1/2 model, described by the Hamiltonian

$$H_{\mathrm{XXZ}} = J \sum_j \left(S_j^x S_{j+1}^x + S_j^y S_{j+1}^y\right) + J_{zz} \sum_j S_j^z S_{j+1}^z$$
$$+ J_{zz}' \sum_j S_j^z S_{j+2}^z, \qquad (7)$$

where S_j^{α} are the standard spin-1/2 operators on site j, J is the hopping amplitude (we set $J = 1$), and we included

interactions between nearest-neighbor spins (J_{zz}) as well as between next-nearest neighbors (J'_{zz}).

For a one-dimensional system like in Eq. (7), in the case $J'_{zz} = 0$, the effect of nearest-neighbor interactions can be rigorously accounted for via integrability techniques [5,12] (in particular, algebraic/coordinate Bethe ansatz) for arbitrary values of J_{zz}. However, integrability is broken as soon as we include interactions between next-nearest-neighbor spins (J'_{zz}), or by generalizing the model to higher dimensions. On the other hand, techniques such as bosonization [48] are very versatile at describing a large class of *gapless* systems that behave as LLs. For the model in Eq. (7) in the absence of J'_{zz} term, the LL phase occurs for $|J_{zz}| < 1$ [49]. Numerical studies using DMRG [28] have shown that the LL phase survives in a finite range of $J'_{zz} > 0$, and is surrounded by two types of charge-density-wave phases and a bond-ordered (BO) phase.

We also remind the reader that the one-dimensional model in Eq. (7) can be directly recast via Jordan-Wigner transformation as a system of spinless fermions hopping on a lattice,

$$
H_{\text{XXZ}} = \frac{J}{2} \sum_j (c_j^\dagger c_{j+1} + \text{H.c.})
$$
$$
+ J_{zz} \sum_j \left(n_j - \frac{1}{2} \right) \left(n_{j+1} - \frac{1}{2} \right)
$$
$$
+ J'_{zz} \sum_j \left(n_j - \frac{1}{2} \right) \left(n_{j+2} - \frac{1}{2} \right), \quad (8)
$$

with nearest-neighbor and next-nearest-neighbor density-density interactions ($n_j \equiv c_j^\dagger c_j$). With antiferromagnetic $J_{zz} > 0$ (and $J'_{zz} = 0$), Eq. (8) captures the low-energy physics of the 1D Fermi-Hubbard model at large interaction U [50]. Thus, even in simple models like in Eqs. (7) or (8), we see that the effects of interactions can be very complex, and lead to a variety of behaviors (gapped or gapless, integrable or nonintegrable, etc.). In the following, we employ the interaction distance and the new concept of integrability distance to numerically investigate the low-energy properties of this system. For smaller system sizes, we use periodic boundary conditions and obtain the ground state numerically using exact diagonalization, resolving the translation symmetry of the system. Alternatively, to access larger system sizes, we assume open boundary conditions and use DMRG method, implemented in ITENSOR [51], to variationally obtain the ground state of the system and its entanglement spectrum. Unless specified otherwise, the entanglement spectrum is obtained by partitioning the system in real space in two subsystems of equal size. As we explained in Sec. II, from the knowledge of the entanglement spectrum, we can efficiently evaluate $D_{\mathcal{F}}$.

IV. QUANTIFYING INTERACTIONS IN THE INTEGRABLE XXZ MODEL

Here we consider the integrable part of H_{XXZ} with $J'_{zz} = 0$. Our aim is to establish how well the interaction distance, $D_{\mathcal{F}}$, can capture the behavior of the model known from its analytical treatment.
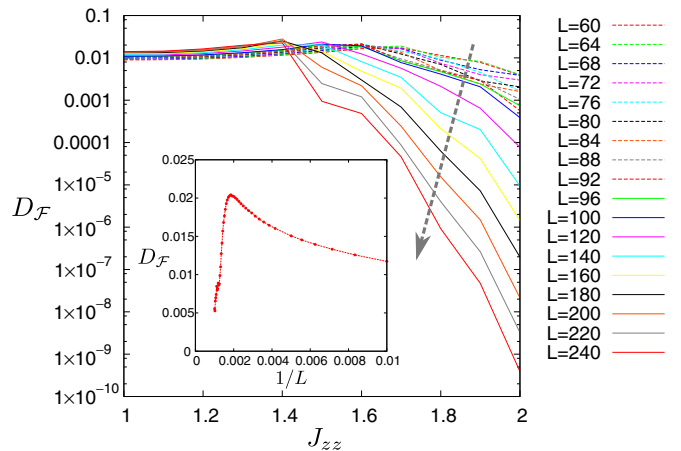

FIG. 2. The interaction distance, $D_{\mathcal{F}}$, in the antiferromagnetic gapped phase of XXZ model with $J_{zz} > 1$, $J'_{zz} = 0$, for various system sizes $L = 4k$. The arrow denotes the decreasing trend of $D_{\mathcal{F}}$ as the system size is increased. Inset shows the finite-size scaling of $D_{\mathcal{F}}$ for the fixed value $J_{zz} = 1.2$ close to the transition.

A. Gapped antiferromagnetic phase of XXZ model

First, we turn our attention to the gapped phase of the integrable XXZ model, i.e., with $J_{zz} > 1$. In Refs. [7,52], it was shown that the reduced density matrix of an infinite system, bipartitioned into two semi-infinite lines, can be written as

$$
\rho_A = \exp \left(- \sum_{j=0,1}^{\infty} \epsilon_j \hat{n}_j \right), \quad \epsilon_j = 2j \ln \left(J_{zz} + \sqrt{J_{zz}^2 - 1} \right),
$$
$$(9)$$

where $\hat{n}_j$ is the fermion number operator, and the sum either starts from $j = 0$ or from $j = 1$. These two choices correspond to the cases with or without spontaneous symmetry breaking [52], i.e., for a doubly degenerate ground state the sum starts with $j = 0$ (and all levels are twofold degenerate), whereas for the symmetry breaking phase (single ground state), the sum starts from $j = 1$. In both cases, the system is evidently free as $\hat{n}_j$ are just free-fermion operators.

We now test the asymptotically emergent free-fermion behavior dictated by Eqs. (9) by numerically calculating $D_{\mathcal{F}}$ for finite size systems. As explained in Sec. III, we use DMRG with open boundary conditions to obtain the entanglement spectrum of the ground state. Unless specified otherwise, we use bond dimension between 400–800 to converge the results. As explained in Ref. [53], the entanglement spectrum is different depending on whether the size of the subsystem is even or odd; in the rest of the paper, we focus on the cases where $L = 4k$, i.e., the subsystem size, typically taken to be half of the total system size, contains an even number of sites, for which entropy is larger [53].

The interaction distance is shown in Fig. 2 for a range of J_{zz} values in the gapped phase and different total system sizes L. From this figure, we see that $D_{\mathcal{F}}$ appears to remain constant where J_{zz} is close to 1, but then starts to exponentially decrease beyond some critical J_{zz}^c. The value of this J_{zz}^c drifts to the left as the system size is increased, which suggests that in the thermodynamic limit, $D_{\mathcal{F}}$ will be zero for any $J_{zz} > 1$.

However, our results also illustrate that one may need to go to very large system sizes in order to start to see the free behavior expected from results of Refs. [7,52]. We see below that this behavior is due to the Berezinskii-Kosterlitz-Thouless (BKT) nature of the phase transition at $J_{zz} = 1$ [54].

To test our previous interpretation of finite size scaling, in the inset of Fig. 2 we pick $J_{zz} = 1.2$, which belongs to the regime where $D_{\mathcal{F}} \approx$ const appears to hold, and then explicitly perform scaling with respect to system size. We see that in small enough systems, $D_{\mathcal{F}}$ typically grows with system size—this is the nonuniversal regime where the system is not big enough to accommodate the dressed DoF due to their large size ℓ. For system sizes greater than some critical value L_c, which is itself a function of J_{zz}, $D_{\mathcal{F}}$ has opposite trend—it decays with system size toward the zero value in an exponential fashion, as we expect from Refs. [7,52]. Thus, we confirm that the integrable XXZ model for $J_{zz} > 1$ can be asymptotically described by free fermions in agreement with Eqs. (9). In other words, the interaction distance $D_{\mathcal{F}}$ reduces to zero as we increase the system size and the optimal free model approaches the free description obtained through integrability methods [7,52]. In particular, for values of $J_{zz} \geqslant 1.5$ and for system sizes larger than $L = 500$, the interaction distance tends to zero, saturating to the value 10^{-8} due to numerical inaccuracies, while the trace distance between the corresponding optimal free model obtained from the interaction distance and the free model given by Eqs. (9) saturates to a value below 10^{-6}.

It is also useful to determine how many entanglement levels are needed to faithfully determine $D_{\mathcal{F}}$. As seen from Eqs. (1) and (2), the interaction distance depends exponentially on the entanglement spectra. Hence, only a small number of entanglement levels is necessary to obtain $D_{\mathcal{F}}$ with a good accuracy. As an example, we consider the interaction distance at $J_{zz} = 2$ and for $L = 600$ and verify that the asymptotic value is already achieved with 25 levels.

B. Gapless Luttinger phase

Next we move on to the gapless LL phase, which is realized in the XXZ model with $|J_{zz}| \leqslant 1$. For this coupling regime, the XXZ model can also be solved via bosonization [48] that maps the low-energy behavior of the system to that of a system of free bosons. Nevertheless, this does not necessitate that the emerging DoF of the model are free bosons. This can be directly verified, e.g., at $J_{zz} = 0$, where the XY model of free fermions emerges, with entanglement spectrum that clearly cannot be described by free bosons. Hence, we continue our investigation in terms of the fermionic interaction distance, $D_{\mathcal{F}}$, across the phase transition to the gapless regime of the LL.

We want to find the behavior of $D_{\mathcal{F}}$ across the phase transition to the gapless regime of the LL. Similar to above, we first scan the behavior of $D_{\mathcal{F}}$ as a function of J_{zz} coupling across the range $0 \leqslant J_{zz} \leqslant 2$ shown in Fig. 3. First, we notice that in the gapped phase $J_{zz} > 1$, the results clearly show the drift of J_{zz}^c toward $J_{zz} = 1$, as discussed previously in Fig. 2. On the other hand, for $J_{zz} < 1$ we are in the LL phase. Intriguingly, we see that for $J_{zz} < 0.4$, $D_{\mathcal{F}}$ exhibits a robust, seemingly linear, growth with J_{zz}. Furthermore, the slope of
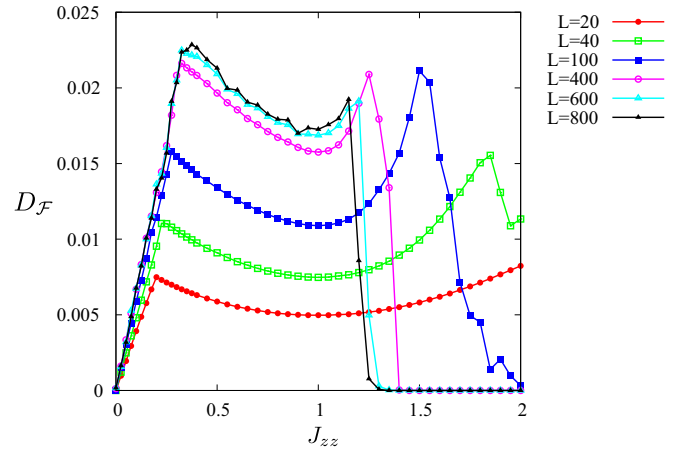

FIG. 3. The interaction distance, $D_{\mathcal{F}}$, as a function of J_{zz} spanning both gapped and gapless regimes. In the gapless regime for small J_{zz}, $D_{\mathcal{F}}$ exhibits a robust linear growth, $D_{\mathcal{F}} \propto J_{zz}$. Data is obtained by DMRG for a sequence of system sizes L indicated in the legend.

the linear growth shows a weak dependence on system size L. More precisely, the slope depends on the size of the *subsystem* L_A, which is fixed at $L_A = L/2$ in Fig. 3.

A simple heuristic argument can explain the growth of $D_{\mathcal{F}}$. Since $D_{\mathcal{F}}$ is predominantly determined by the largest eigenvalues of ρ_A or, equivalently, the lowest entanglement energies, it is important to know the low-lying structure of the entanglement spectrum in the LL phase. A general theorem by Bisognano and Wichmann [55,56], applicable to systems described by relativistic quantum field theory, establishes a direct correspondence between the eigenvalues of ρ_A and the energy eigenvalues of the Hamiltonian restricted to the subsystem [57–59]. Thus, for $|J_{zz}| < 1$, the entanglement energies are given by the actual energies of a LL Hamiltonian for open boundary conditions. The Hamiltonian of a LL with open boundary condition is given, e.g., in Eq. (129) of Ref. [54],

$$H = \sum_{q>0} \hbar v \, q \, a_q^\dagger a_q + \frac{\hbar \pi v}{2LK}(\hat{N} - N)^2, \qquad (10)$$

where v is the velocity, K is the Luttinger parameter, L denotes the system size, and $\hat{N}$ is the total number operator. For XXZ model, Bethe ansatz gives explicit expressions for v and K [54],

$$v = \frac{\pi v_F}{2} \frac{\sqrt{1 - J_{zz}^2}}{\arccos J_{zz}},$$

$$K = \frac{1}{2 - \frac{2}{\pi}\arccos J_{zz}}, \qquad (11)$$

where $v_F = 1$ for $J = 1$. Generally, K and v can be treated as phenomenological parameters. Since the LL Hamiltonian has a U(1) symmetry, the spectrum splits into different number sectors with a parabolic envelope given by the second term in the Hamiltonian. In addition, for fixed N, the first term in the Hamiltonian gives the spectrum of bosons, with the tower of states whose degeneracies are equal to the number
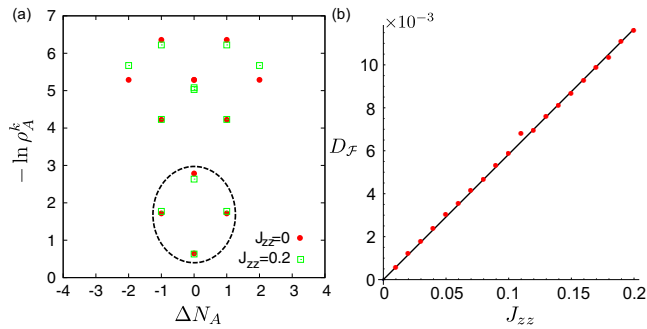
FIG. 4. (a) Entanglement spectrum of the ground state of XXZ model with $J_{zz} = 0$ (XY model) and $J_{zz} = 0.2$. Data is for system size $L = 24$ obtained by exact diagonalization. Entanglement energies, $-\ln \rho_k$, are plotted as a function of the number of particles in A subsystem. The four lowest levels (indicated by the dashed circle) are responsible for the increase in $D_{\mathcal{F}}$ with J_{zz}. Comparing the case $J_{zz} = 0$ with that of $J_{zz} = 0.2$, we see that the symmetry of the four levels around the middle point [cf. Eq. (5)] gets destroyed in the presence of interactions, as the topmost level slightly comes down, while the two degenerate ones move upward. (b) The linear growth of $D_{\mathcal{F}}$ as a function of J_{zz} obtained from DMRG is compared against the analytic ansatz in Eq. (15), with $\ell_0 \approx 4.6$ and system size $L = 100$.

of partitions of an integer, i.e., the degeneracies are 1, 1, 2, 3, 5, 7, etc.

The universality of the LL Hamiltonian implies that the general structure of its energy levels directly translates into the same structure of the *entanglement energies* for the subsystem's reduced density matrix. The analysis of the entanglement spectrum from this point of view was performed in detail in Ref. [60], and we reproduce an example in Fig. 4(a) for a small XXZ periodic chain of $L = 24$ spins with $J_{zz} = 0$ and $J_{zz} = 0.2$. The entanglement spectrum in Fig. 4(a) is plotted as a function of ΔN_A, the relative number of particles in the subsystem A compared to $N_A = N/2$. The spectrum splits into conformal towers corresponding to different particle numbers, $\Delta N_A = 0, \pm 1, \pm 2, \ldots$. The behavior of $D_{\mathcal{F}}$ as a function of J_{zz} can be explained by considering the lowest four entanglement energies, which have been indicated by a dashed circle in Fig. 4(a). From the form of the Hamiltonian in Eq. (10) (assuming Dirichlet boundary conditions), we see that these entanglement energies are given by

$$
\begin{aligned}
E_0 &= e_0, \\
E_1 = E_2 &= e_0\left(1 + \frac{1}{2K}\right), \\
E_3 &= 2e_0.
\end{aligned}
\tag{12}
$$

with $e_0 = \frac{\pi \hbar v}{L}$, i.e., two of them are in the sector with half the number of particles in A ($\Delta N_A = 0$), and two remaining energies are in number sectors that differ by ± 1. We have compared these energy levels with the behavior of the levels obtained numerically from the entanglement Hamiltonian and we found excellent agreement.

From Eqs. (12), it is clear why $D_{\mathcal{F}}$ increases: When $K = 1$ (XY model), the four levels are symmetric around the midpoint ($E_{\max} + E_{\min}$)/2, thus describable by the free-fermion modes as in Eq. (5) and $D_{\mathcal{F}} = 0$; in all other cases, we obtain

a set of four entanglement energies that are not symmetric around the middle point and thus cannot be described by Eq. (5). Hence, $D_{\mathcal{F}}$ is not zero and can be precisely quantified. For small J_{zz}, we can assume the corresponding free model is just the XY model, for which the (unnormalized) reduced density matrix eigenvalues are $\sigma_0 = 1$, $\sigma_1 = \sigma_2 = e^{-\beta_{\text{ent}}/2}$, $\sigma_3 = e^{-\beta_{\text{ent}}}$. The interaction distance is then given by

$$
D_{\mathcal{F}} = \frac{1}{2} \sum_{k=0}^{3} \left| \frac{1}{Z} e^{-\beta_{\text{ent}} E_k} - \frac{1}{Z_\sigma} \sigma_k \right|,
\tag{13}
$$

which can be evaluated using Eqs. (12). Note that the (inverse) entanglement temperature β_{ent} should be set (for an open system) according to [61]

$$
\beta_{\text{ent}} = \frac{2\pi L_A}{v \ln(L_A/\ell_0)},
\tag{14}
$$

where ℓ_0 is a lattice regularization. The latter can be found, e.g., from the bipartite fluctuation of magnetization [61]. Note that the final result for $D_{\mathcal{F}}$ involves products of the form $\beta_{\text{ent}} E_k$. Hence, it continues to carry a weak subsystem-size dependence via the factor $\ln(L_A/\ell_0)$ from the definition of entanglement temperature.

Using the expressions in Eqs. (13), (14), and (11), and expanding to first order in J_{zz}, we obtain

$$
D_{\mathcal{F}} = J_{zz} \frac{3\pi \cosh\left(\pi^2 / \ln \frac{L_A}{\ell_0}\right)}{8 \ln \frac{L_A}{\ell_0} \cosh^4\left(\pi^2 / \left(2 \ln \frac{L_A}{\ell_0}\right)\right)} + \mathcal{O}(J_{zz}^2).
\tag{15}
$$

Using, e.g., $\ell_0 \approx 4.6$, this formula gives a good agreement against the $D_{\mathcal{F}}$ growth calculated in DMRG for a system of $L = 100$ sites, as shown in Fig. 4(b). Hence, it is possible to faithfully determine the behavior of $D_{\mathcal{F}}$ from a small number of lowest eigenvalues even if the system is in the gapless regime. We note that, unlike the gapped phase which was studied in Refs. [7,52], we are unaware of analytical results for the entanglement spectrum in the LL phase in the limit of an infinite system.

Finally, it is interesting to analyze what happens when our simple toy model in Eqs. (12) is pushed beyond its validity when system size L becomes very large. In this case, the structure of the entanglement spectrum will change, with an increasing number of entanglement levels becoming degenerate with each other. This is because of weak logarithmic dependence of entanglement temperature on the subsystem size, as noted above. Thus, based on our simple toy model, we may expect that there is a crossover between the linear increase of $D_{\mathcal{F}}$ to a decay in much larger system sizes. Such a result would be in agreement with the expectation from Baxter's analysis that any integrable system in the critical or noncritical regime is faithfully described by free fermions. A full numerical verification of this result is currently out of our reach: The large system sizes required to approach the thermodynamic limit make the accurate evaluation of $D_{\mathcal{F}}$ formidable. An investigation with dedicated numerical recipes for the accurate evaluation of interaction distance for large system sizes will be carried out in a future work.
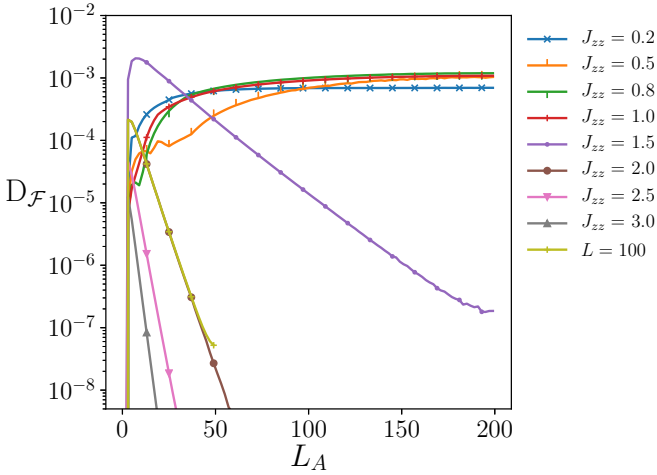
FIG. 5. The interaction distance, $D_\mathcal{F}$, plotted on a logarithmic scale as a function of subsystem size L_A, on the integrable line $J'_{zz} = 0$ for various J_{zz}. Total size of the chain is fixed at $L = 400$ sites, with an additional data point at $L = 100$ $J_{zz} = 2$. We see that in the entire Luttinger liquid phase ($J_{zz} \leqslant 1$), there is no decay of $D_\mathcal{F}$ with subsystem size L_A. On the other hand, in the gapped antiferromagnetic phase, $D_\mathcal{F}$ decays exponentially with L_A, with an exponent that depends on J_{zz}. This decay reflects the exponential localization of fermionic dressed DoF, that does not change with system size.

C. Probing the structure of dressed DoF

From the previous analysis we have seen that the XXZ model has $D_\mathcal{F} \to 0$ as $L \to \infty$, for $J_{zz} > 1$. This reflects the fact that the dressed DoF of the model tend to behave like free fermions even for finite but large system sizes, extending the infinite size result of Eqs. (9). Note that the internal structure of the dressed DoF is generated from the interactions due to a nontrivial rotation $U c_j U^\dagger$. Nevertheless, for large enough system sizes and partitions L_A, the fermionic dressed DoF fit well within the region of the partition L_A and its complement, as shown in Fig. 1(a). Then the interaction distance measures the free particle correlations giving $D_\mathcal{F} \approx 0$, as shown in Fig. 2. When L_A becomes small compared to the size, ℓ, of the dressed DoF, then the lowest part of the resulting entanglement spectrum will be influenced by the structure of the dressed DoF, as shown in Fig. 1(b). The part of the entanglement spectrum that corresponds to the internal structure of the quasiparticles does not necessarily correspond to free correlations as the structure of U comes from the presence of interactions. This is precisely the information about the dressed DoF that can be captured by $D_\mathcal{F}$.

We can quantitatively extract the size of the dressed DoF of the XXZ model by examining the dependence of $D_\mathcal{F}$ on the subsystem size, L_A, for various choices J_{zz} in the gapped and gapless regions. In this analysis, we keep the total size of the system fixed at $L = 400$. This size is large enough to be in the proper scaling regime, giving $D_\mathcal{F} \to 0$ for many choices of $J_{zz} \gtrsim 1.5$. In Fig. 5, we vary the location of the partition for fixed system size. We see that there is an exponential increase in $D_\mathcal{F}$ when the subsystem size is reduced down to $L_A \sim 20$, then it goes identically to zero $D_\mathcal{F} = 0$ for $L_A = 1$, as calculated analytically [3]. This increase can be explained in
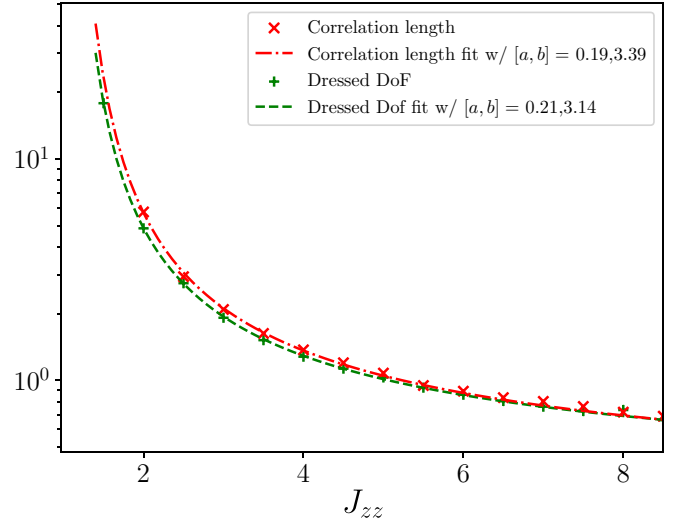

FIG. 6. Numerically determined size ℓ of the dressed DoF and correlation length ξ as a function of J_{zz}. Both data points are fit according to Eq. (19), with the critical value $J^c_{zz} = 1$. Both ℓ and the ξ diverge with roughly the same functional form and $\ell \sim \xi$.

terms of Fig. 1 that depicts localized dressed DoF. Assuming that the profile of the dressed DoF is exponential, we expect the scaling behavior of $D_\mathcal{F}$ to be given by

$$D_\mathcal{F} \propto \exp(-L_A/\ell). \quad (16)$$

From this relation, we can extract the size ℓ of the dressed DoF as a function of J_{zz}, as shown in Fig. 6. We compare its divergence with the divergence of the correlation length ξ as the system approaches the critical point at $J^c_{zz} = 1$. The correlation length is extracted from the spin-spin correlations,

$$G(r) = \langle S^z_j S^z_{j+r} \rangle - \langle S^z_j \rangle \langle S^z_{j+r} \rangle, \quad (17)$$

using an exponential fit with a polynomial prefactor [62]:

$$G(r) \sim \frac{1}{r^2} e^{-r/\xi}. \quad (18)$$

It was recently pointed out [63] that using a simple exponential instead of the correct Ornstein-Zernike ansatz as in Eq. (18) would result in large errors for the estimated ξ. From the fit to Eq. (18), we find divergence of the correlation length as J_{zz} approaches the critical point, as shown in Fig. 6. The divergence takes the form characteristic of the BKT transition [54],

$$f(J_{zz}) = a \exp\left(\frac{b}{\sqrt{|J_{zz} - J^c_{zz}|}}\right), \quad (19)$$

with constant a and b. Surprisingly, as we observe in Fig. 6, ℓ also diverges with J_{zz} in a similar fashion to ξ. This signals that in the present case they both depend on the energy gap of the system according to

$$\ell \sim \xi \sim E^{-1}_{\text{gap}} \quad (20)$$

within the gapped phase. The fitting parameters are $[a, b] = [0.19, 3.39], [0.21, 3.14]$ for ξ and ℓ, respectively, when fit to the critical point at $J^c_{zz} = 1$. The value of b for ξ and ℓ are

found to be within 3% and 10% of the asymptotic Bethe ansatz result [26].

The exponential profile in $D_{\mathcal{F}}$ shows that the effective DoF are dressed by interactions with an exponential tail. As J_{zz} is tuned away from J_{zz}^c in the gapped phase, the dressed DoF move toward a single particle picture, with $J_{zz} \to \infty$ trivially free. Indeed, at that point one would find the interaction distance identically zero $D_{\mathcal{F}} = 0$ for all choices of cut as it is possible, via a Jordan-Wigner transformation, to map the interacting Hamiltonian to one that is quadratic in its fermionic operators. Thus, the dressed DoF size ℓ is also trivially zero at this point. Within the LL phase, we see in Fig. 5 no exponential profile attached to $D_{\mathcal{F}}$ as the partition is changed. So it is not possible to extract a meaningful, finite size ℓ due to the critical nature of this phase.

V. QUANTIFYING INTERACTIONS IN THE NONINTEGRABLE REGIME

Our previous analysis on the XXZ model complements the rigorously established results in the literature, obtained either by Bethe ansatz or bosonization techniques, and calibrates $D_{\mathcal{F}}$ on an integrable model. Now we investigate the effect of next-nearest-neighbor interactions, $J_{zz}' \neq 0$, which break the integrability of the model.

A. Interaction distance of the extended XXZ model

Previous numerical studies of the extended XXZ model using DMRG [28] have mapped out its phase diagram as a function of J_{zz} and J_{zz}'. It was established that the phase diagram consists of four phases: the LL phase, two types of charge-density wave (CDW1, CDW2) phases, and a BO phase.

In Fig. 7, we map out the phase diagram J_{zz}-J_{zz}' based on the value of $D_{\mathcal{F}}$ in the ground state. Although the phase diagram in Fig. 7 is obtained for a rather small system size ($L = 20$, with periodic boundary conditions), its structure is broadly consistent with phase boundaries found in Ref. [28], indicated by dashed lines. In particular, the structure of $D_{\mathcal{F}}$ clearly reveals the presence of at least four different phases. The LL phase is dominated by the larger values of $D_{\mathcal{F}}$ as it corresponds to a gapless phase, compared to the gapped charge-density-wave phases. Indeed, when the energy gap is small then the corresponding ground state is more susceptible to the presence of interactions and $D_{\mathcal{F}}$ is large. However, this is not true near the origin of the phase diagram where we see a semicircular lobe with small values of $D_{\mathcal{F}}$. On the integrable line $J_{zz}' = 0$, this lobe corresponds to the regime of linear increase of $D_{\mathcal{F}}$ that we discussed in Fig. 3, and we expect that a similar behavior persists when a small amount of J_{zz}' is added.

Beside the LL phase, there are also three ordered phases in the phase diagram in Fig. 7. The crystalline phases CDW1 and CDW2 have a simple interpretation in the classical ("atomic") limit when the XY term in the Hamiltonian is completely switched off. In that limit, CDW1 is adiabatically connected to the degenerate Néel product states, $101010\ldots$ and $010101\ldots$, while CDW2 has a doubled unit cell, $110011001100\ldots$ (and translated copies). Finally, the
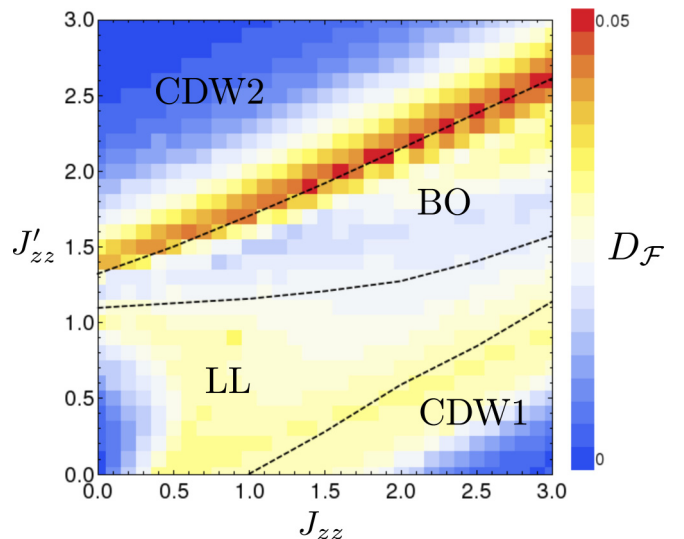

FIG. 7. Interaction distance $D_{\mathcal{F}}$ (color scale) across the 2D phase diagram J_{zz}-J_{zz}' for system size $L = 20$ with periodic boundary conditions, obtained by exact diagonalization. Dashed lines are approximate phase boundaries reproduced from Ref. [28], which separate the following phases: gapless Luttinger liquid phase (LL), two types of charge density wave phases (CDW1 and CDW2), and a bond ordered phase (BO).

BO phase [64] is defined by the finite value of the order parameter, $\langle \frac{1}{L} \sum_i (-1)^i (c_i^\dagger c_{i+1} + h.c.) \rangle$. All these phases, being weakly correlated, are expected to have relatively low values of $D_{\mathcal{F}}$, as indeed confirmed by Fig. 7.

We now investigate the scaling behavior of $D_{\mathcal{F}}$ as we change the partition size L_A. From Eq. (16), we can extract size ℓ of the dressed DoF as we did for the integrable XXZ model. Figure 8 shows that size ℓ behaves similarly to the correlation length ξ as it approaches the phase transition from the charge-density-wave phase to the LL phase. Both ℓ and ξ have a scaling behavior consistent with BKT phase transition [26]; however, there is a small deviation between their values in comparison to the integrable XXZ case.

B. Integrability distance

Finally, we are interested in the gapless LL phase of the extended XXZ model. As we have seen in Fig. 7, in small system sizes $D_{\mathcal{F}}$ has a nonmonotonic behavior in this phase, which motivates us to search for a more robust diagnostic. The form of the extended XXZ Hamiltonian and our analysis so far suggest we introduce the following "distance," instead of $D_{\mathcal{F}}$, to quantitatively investigate the LL phase:

$$D_{\text{XXZ}}(\rho) = \min_{-1 \leqslant J_{zz} \leqslant 1} \frac{1}{2} \text{tr} \sqrt{(\rho - \sigma(J_{zz}))^2}. \quad (21)$$

Here ρ is the reduced density matrix of the extended XXZ model and the minimization is over $\sigma(J_{zz})$ which represents the reduced density matrix of the XXZ ground state at $-1 \leqslant J_{zz} \leqslant 1$ ($J_{zz}' = 0$). Unlike the definition of $D_{\mathcal{F}}$ in Eq. (1), note that $\sigma(J_{zz})$ is *not* necessarily a free-fermion density matrix, but that of the integrable XXZ model. Furthermore, we have used quotes in the name distance because D_{XXZ} characterizes correlations in a single quantum state, rather than the spectral
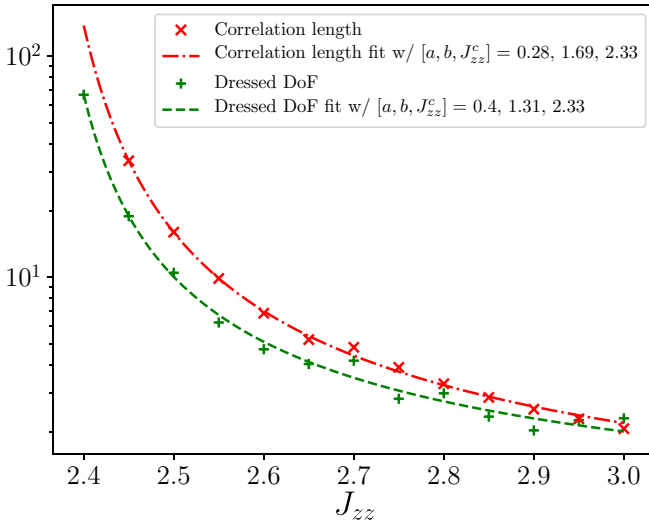
FIG. 8. Numerically determined size ℓ of the dressed DoF and correlation length ξ as a function of J_{zz} for the line $J'_{zz} = 3 - J_{zz}$, i.e., approaching the LL-CDW1 phase transition from within the gapped phase in Fig. 7. Data points are fit using the ansatz in Eq. (19), with the critical value extracted as $J^c_{zz} = 2.33$. Both ℓ and the ξ diverge with the same functional form signaling that the phase transition LL-CDW1 in the extended model is also of BKT type.

properties of the entire Hamiltonian (although the two should be linked in some way). In general, a more appropriate quantity would be the *integrability distance*, $D_\mathcal{I}$, defined as

$$D_\mathcal{I}(\rho) = \min_{\sigma \in \mathcal{I}} \tfrac{1}{2} \mathrm{tr} \sqrt{(\rho - \sigma)^2}, \qquad (22)$$

where the minimization is performed over the set of all integrable models, $\mathcal{I}$. Several difficulties arise with this distance as explained below. For our immediate purposes, given the form of the extended XXZ Hamiltonian, it seems natural to measure how far it is from the XXZ model in the Luttinger phase and hence to restrict our attention to D_{XXZ}.

In practice, we evaluate D_{XXZ} numerically by precomputing $\sigma(J_{zz})$ for a dense set of values J_{zz} distributed in the interval $[-1, 1]$. Then, for every value of the parameters (J_{zz}, J'_{zz}), we obtain the ground state of the system, find its reduced density matrix ρ, and identify which of the precomputed $\sigma(J^*_{zz})$ minimizes the trace distance in Eq. (22). This gives us two bits of information: (i) we obtain the optimal LL coupling J^*_{zz} on the integrable line or, equivalently, the effective Luttinger parameter K^* given by Eq. (11) [48], which best approximates the ground state at a *non-integrable* point (J_{zz}, J'_{zz}); and (ii) we also obtain information about the quality of the approximation from the minimal achieved trace distance between ρ and $\sigma(J^*_{zz})$. If this minimal trace is not close to zero, the approximation is poor, and the description in terms of an integrable LL is not useful. Compared with the results, e.g., of Ref. [19] for the effective value of the Luttinger parameter K^* along the cut $J'_{zz} = 2J_{zz} - 2.5$, we found that the optimal integrable model has K^* that is in good agreement, with at most a 6% deviation.

In Fig. 9, we evaluate D_{XXZ} for the extended XXZ model by varying both interactions, J_{zz} and J'_{zz}. Figure 9(a) shows the optimal integrable Luttinger coupling J^*_{zz} for each
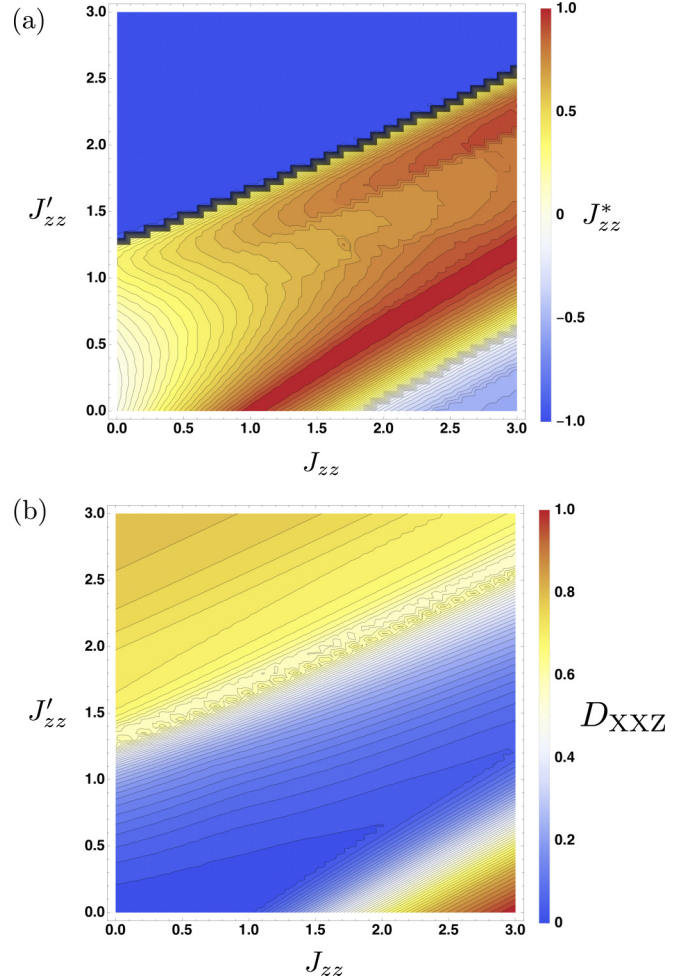

FIG. 9. Integrability distance D_{XXZ} across the two-dimensional phase diagram J_{zz}-J'_{zz}. Data is obtained by exact diagonalization for system size $L = 20$. Panel (a) shows the optimal integrable Luttinger coupling J^*_{zz} for each point (J_{zz}, J'_{zz}) in the phase diagram, with the corresponding minimal trace distance shown in panel (b). We see that the trace distance is small only in the diagonal strip of the phase diagram, which is consistent with the region identified as the LL phase in Ref. [28].

point (J_{zz}, J'_{zz}) in the phase diagram, with the corresponding minimal trace distance shown in Fig. 9(b). Indeed, from J^*_{zz}, the parameters K and v in Eq. (11) can be fully determined that give the Hamiltonian of the LL, Eq. (10), that best approximates the model at that point in the phase diagram. We see that the trace distance is small only in the diagonal strip of the phase diagram, which is consistent with the region identified as the LL phase in Ref. [28]. Outside of this region, our optimal model is not accurate. Interestingly, along the phase boundary of the LL-CDW1 transition, we find that the optimal model is $J^*_{zz} = 1$. This is consistent with the literature [28] which found that the Luttinger parameter K along the entire phase boundary assumes the value $K^* = \frac{1}{2}$ (which translates to our $J^*_{zz} = 1$).

VI. CONCLUSIONS AND OUTLOOK

In this paper, we qualitatively and quantitatively investigated the behavior of the extended XXZ model, focusing on the effect of interactions on different phases. This model has an integrable line that we probed with the interaction distance, $D_{\mathcal{F}}$. In the gapped regime, we investigated the behavior of its effective DoF, dressed by the interactions, that naturally emerge through the scaling analysis of the interaction distance. Hence, the interaction distance can efficiently describe the short- and long-distance behavior of the model. Moreover, we provided analytical arguments about the behavior of the interaction distance, $D_{\mathcal{F}}$, in the gapless LL regime of the integrable XXZ model.

Outside the integrable line, a large part of the phase diagram of the extended XXZ model is expected to be described by the LL. The investigation of this property motivates the introduction of the concept of integrability distance, $D_{\mathcal{I}}$ as in Eq. (22). Similar to the interaction distance, ρ in Eq. (22) can represent the Boltzmann-Gibbs density matrix of the system or it can be the reduced density matrix of any eigenstate of the system, when it is bipartitioned. In this way, ρ can systematically probe all the relevant properties of integrable systems such as their energy spectrum and their quantum correlations. Moreover, $D_{\mathcal{I}}$ could be directly expressed with respect to the eigenvalues of ρ and σ. Nevertheless, two fundamental difficulties arise when working with Eq. (22). One

is that, unlike the free-fermion density matrices, the general structure for σ of integrable systems is not known. Another is that the set $\mathcal{I}$ of all possible integrable models one can envisage is not completely understood. In practice, one could simply list all the models that are known to be integrable up to now and run over this set. Due to the formidable complexity of varying over the whole space $\mathcal{I}$ of integrable models, we leave the investigation of the integrability distance, Eq. (22), to future work. Identifying the general structure of σ for (at least some) integrable models would be an important step. It would allow us to evaluate $D_{\mathcal{I}}$ in full generality and thus help to quantitatively demonstrate how close nonintegrable but physically relevant models are to mathematically idealized integrable examples. In view of these points, in our case, we restricted our attention to D_{XXZ} to quantitatively demonstrate that the extended XXZ model can be faithfully described by the LL with good accuracy. That being said, using $D_{\mathcal{I}}$, one could well imagine that at those points in the parameter space J_{zz}-J'_{zz}, where D_{XXZ} is not small, the extended XXZ model is in fact "closer to" another integrable model.

In compliance with EPSRC policy framework on research data, this publication is a theoretical work that does not require supporting research data.

[1] E. M. Lifshitz, L. D. Landau, and L. P. Pitaevskii, *Statistical Physics, Part 2: Theory of the Condensed State* (Pergamon Press, 1980).

[2] B. Sutherland, *Beautiful Models: 70 Years of Exactly Solved Quantum Many-body Problems* (World Scientific, 2004).

[3] C. J. Turner, K. Meichanetzidis, Z. Papic, and J. K. Pachos, Nat. Commun. **8**, 14926 (2017).

[4] H. Li and F. D. M. Haldane, Phys. Rev. Lett. **101**, 010504 (2008).

[5] R. J. Baxter, *Exactly Solved Models in Statistical Mechanics* (Elsevier, 1982).

[6] T. Nishino, J. Phys. Soc. Jpn. **64**, 3598 (1995).

[7] I. Peschel, M. Kaulke, and O. Legeza, Ann. Phys. **8**, 153 (1999).

[8] I. Peschel and M.-C. Chung, J. Phys. A: Math. Gen. **32**, 8419 (1999).

[9] I. Peschel, J. Stat. Mech.: Theory Exp. (2004) P06004.

[10] S.-i. Tomonaga, Prog. Theore. Phys. **5**, 544 (1950).

[11] J. M. Luttinger, J. Math. Phys. **4**, 1154 (1963).

[12] M. Gaudin, *The Bethe Wavefunction* (Cambridge University Press, 2014).

[13] V. E. Korepin, N. M. Bogoliubov, and A. G. Izergin, *Quantum Inverse Scattering Method and Correlation Functions*, Cambridge Monographs on Mathematical Physics (Cambridge University Press, 1993).

[14] J.-S. Caux, J. Math. Phys. **50**, 095214 (2009).

[15] S. R. White, Phys. Rev. Lett. **69**, 2863 (1992).

[16] U. Schollwöck, Ann. Phys. **326**, 96 (2011), January 2011 Special Issue.

[17] G. Vidal, Phys. Rev. Lett. **98**, 070201 (2007).

[18] D. Peters, I. P. McCulloch, and W. Selke, Phys. Rev. B **85**, 054423 (2012).

[19] P. Schmitteckert and U. Eckern, Phys. Rev. B **53**, 15397 (1996).

[20] S. Ejima, F. Gebhard, and S. Nishimoto, Europhys. Lett. **70**, 492 (2005).

[21] R. G. Pereira, S. R. White, and I. Affleck, Phys. Rev. Lett. **100**, 027206 (2008).

[22] R. G. Pereira, S. R. White, and I. Affleck, Phys. Rev. B **79**, 165113 (2009).

[23] E. Jeckelmann, J. Phys.: Condens. Matter. **25**, 014002 (2012).

[24] C. Karrasch and J. E. Moore, Phys. Rev. B **86**, 155156 (2012).

[25] A. K. Zhuravlev and M. I. Katsnelson, Phys. Rev. B **61**, 15534 (2000).

[26] P. Schmitteckert and R. Werner, Phys. Rev. B **69**, 195115 (2004).

[27] C.-B. Duan and W.-Z. Wang, J. Phys.: Condens. Matter. **23**, 365602 (2011).

[28] T. Mishra, J. Carrasquilla, and M. Rigol, Phys. Rev. B **84**, 115135 (2011).

[29] B. Dóra, R. Lundgren, M. Selover, and F. Pollmann, Phys. Rev. Lett. **117**, 010603 (2016).

[30] C. Karrasch, J. Rentrop, D. Schuricht, and V. Meden, Phys. Rev. Lett. **109**, 126406 (2012).

[31] J. K. Pachos and Z. Papic, Sci. Post. Phys. Lect. Notes, 4 (2018), doi:10.21468/SciPostPhysLectNotes.4.

[32] M. A. Nielsen and I. L. Chuang, *Quantum Computation and Quantum Information: 10th Anniversary Edition*, 10th ed. (Cambridge University Press, New York, 2011).

[33] H. Casini, M. Huerta, and R. C. Myers, J. High Energy Phys. 05 (2011) 036.

[34] J. Cardy and E. Tonni, J. Stat. Mech.: Theory Exp. (2016) 123103.

[35] X.-L. Qi, H. Katsura, and A. W. W. Ludwig, Phys. Rev. Lett. **108**, 196402 (2012).

[36] D. Markham, J. A. Miszczak, Z. Puchała, and K. Życzkowski, Phys. Rev. A **77**, 042111 (2008).

[37] K. Meichanetzidis, C. J. Turner, A. Farjami, Z. Papić, and J. K. Pachos, Phys. Rev. B **97**, 125104 (2018).

[38] M. G. Genoni, M. G. A. Paris, and K. Banaszek, Phys. Rev. A **78**, 060303(R) (2008).

[39] J. S. Ivan, M. S. Kumar, and R. Simon, Quant. Info. Proc. **11**, 853 (2012).

[40] G. Adesso, S. Ragy, and A. R. Lee, Open Syst. Inform. Dyn. **21**, 1440001 (2014).

[41] P. Marian and T. A. Marian, Phys. Rev. A **88**, 012322 (2013).

[42] C. Weedbrook, S. Pirandola, R. García-Patrón, N. J. Cerf, T. C. Ralph, J. H. Shapiro, and S. Lloyd, Rev. Mod. Phys. **84**, 621 (2012).

[43] J. Gertis, M. Friesdorf, C. A. Riofrío, and J. Eisert, Phys. Rev. A **94**, 053628 (2016).

[44] L. Vanderstraeten, J. Haegeman, T. J. Osborne, and F. Verstraete, Phys. Rev. Lett. **112**, 257202 (2014).

[45] L. Vanderstraeten, F. Verstraete, and J. Haegeman, Phys. Rev. B **92**, 125136 (2015).

[46] L. Vanderstraeten, *Tensor Network States and Effective Particles for Low-Dimensional Quantum Spin Systems*, Springer Theses (Springer International Publishing, 2017).

[47] E. Lieb, T. Schultz, and D. Mattis, Ann. Phys. **16**, 407 (1961).

[48] A. O. Gogolin, A. A. Nersesyan, and A. M. Tsvelik, *Bosonization and Strongly Correlated Systems* (Cambridge University Press, 2004).

[49] T. Giamarchi and O. U. Press, *Quantum Physics in One Dimension*, International Series of Monographs on Physics (Clarendon Press, 2004).

[50] F. H. Essler, H. Frahm, F. Göhmann, A. Klümper, and V. E. Korepin, *The One-Dimensional Hubbard model* (Cambridge University Press, 2005).

[51] ITensor Library (version 2.0.11), http://itensor.org.

[52] V. Alba, P. Calabrese, and E. Tonni, J. Phys. A: Math. Theor. **51**, 024001 (2017).

[53] N. Laflorencie, E. S. Sørensen, M.-S. Chang, and I. Affleck, Phys. Rev. Lett. **96**, 100603 (2006).

[54] M. A. Cazalilla, R. Citro, T. Giamarchi, E. Orignac, and M. Rigol, Rev. Mod. Phys. **83**, 1405 (2011).

[55] J. J. Bisognano and E. H. Wichmann, J. Math. Phys. **16**, 985 (1975).

[56] J. J. Bisognano and E. H. Wichmann, J. Math. Phys. **17**, 303 (1976).

[57] B. Swingle and T. Senthil, Phys. Rev. B **86**, 045117 (2012).

[58] M. Goldstein and E. Sela, Phys. Rev. Lett. **120**, 200602 (2018).

[59] G. Giudici, T. Mendes-Santos, P. Calabrese, and M. Dalmonte, Phys. Rev. B **98**, 134403 (2018).

[60] A. M. Läuchli, arXiv:1303.0741.

[61] N. Laflorencie and S. Rachel, J. Stat. Mech.: Theory Exp. (2014) P11013.

[62] M. Dugave, F. Göhmann, K. K. Kozlowski, and J. Suzuki, J. Stat. Mech.: Theory Exp. (2015) P05037.

[63] M. M. Rams, P. Czarnik, and L. Cincio, Phys. Rev. X **8**, 041033 (2018).

[64] K. Hallberg, E. Gagliano, and C. Balseiro, Phys. Rev. B **41**, 9474 (1990).